Available online at www.sciencedirect.com
SCIENCE DIRECT®
Remote Sensing of Environment 88 (2003) 221–232
Remote Sensing of Environment
www.elsevier.com/locate/rse

Comparison of BRDF models with a fuzzy inference system for correction of bidirectional effects

Ross Bryant[a,*], Jiaguo Qi[b], M. Susan Moran[a], Wanmei Ni[a]

[a] USDA, Agricultural Research Service, Southwest Watershed Research Center, 2000 East Allen Road, Tucson, AZ 85719, USA
[b] Center for Global Change and Earth Observations and Department of Geography, Michigan State University, 1405 S. Harrison Road, Room 101 Manly Miles Building, East Lansing, MI 48823, USA

Received 10 July 2002; received in revised form 3 March 2003; accepted 8 March 2003

Abstract

With the advances in computing and imaging technology, the field of precision agriculture is rapidly becoming a practical means for farm management. An important step in the delivery of highly accurate images for farm managers is the within-image correction for viewing geometry effects. Reflected light on an imaging sensor is influenced by properties of view zenith angle, solar zenith angle, and relative azimuth. There are a number of models that describe this effect termed the bidirectional reflectance distribution function (BRDF) or more generically "viewing geometry effects." In this paper, we compared three BRDF models (Roujean, Shibayama–Wiegand, and Dymond–Qi) with a fuzzy inference system (FIS) for three data sets for correction of geometric effects. One data set consisted of ground data collected at different viewing angles of a cotton crop. Another data set included six aircraft images of a corn plot in a different part of each image. The final data set was an aerial image of a planting density experiment of cotton. All the models performed reasonably well, but the FIS was the most consistent predictor of BRDF for all three data sets. For the ground data set, R^2 statistics for predicting the reflectance based on the trained models ranged from 0.53 to 0.93 for the BRDF models and from 0.94 to 0.97 for the FIS.

Keywords: BRDF models; Fuzzy inference system; Bidirectional effects

1. Introduction

Remote sensing for precision agriculture is on the verge of becoming an extremely valuable tool for the farming industry. The combination of investments in satellites dedicated specifically to acquisition of images for the agriculture industry and advances in geographic information science and computer technology will make precision agriculture a common practice. Just as the industrial age saw the mechanization of agriculture, the information age will usher in spatially explicit, knowledge-based agriculture.

This new agriculture will rely on accurate information obtained from sophisticated instruments mounted on farm machinery, airplanes, and satellites. In many cases, the information from the air will be image-based; that is, agricultural professionals will obtain information about their fields from a "picture" of their farm made of an array of numbers, with each number corresponding to a precise point (pixel) in the field. To produce an information-rich map of a crop, the image needs to be corrected for differences arising from the interaction of the illumination source of the image and the pixel location within the image due to the bidirectional nature of most agricultural fields. In this paper, these differences are referred to as "viewing geometry effects" because the effect is primarily related to geometric configuration of the sensing system.

The need to correct for viewing geometry effects has been recognized ever since remote sensing has been used for scientific, quantitative purposes (Asrar & Myneni, 1992; Deering, Eck, & Otterman, 1990; Kimes, Sellers, & Diner, 1987; Qi, Huete, Moran, Chehbouni, & Jackson, 1993). Only in the past decade have the computing tools been available to make the correction practical for large images. Many bidirectional reflectance distribution function (BRDF) models have been developed to correct for this effect (e.g., Strahler, 1997). Some of these models have been validated (Hu,

* Corresponding author. Tel.: +1-520-670-6380; fax: +1-520-670-5550.
E-mail address: rbryant@tucson.ars.ag.gov (R. Bryant).

0034-4257/$ - see front matter © 2003 Elsevier Inc. All rights reserved.
doi:10.1016/S0034-4257(03)00072-5

Table 1
Data acquisition sites

Sites	Type of data	Date of acquisition
Lubbock, TX	ground data	July 20 1998, 8:00 a.m.
	aircraft data	June 26 1998, 9:00 a.m.
Shafter, CA	aircraft data	May 27 1997, 11:00 a.m.

Wanner, & Strahler, 1997) and are currently used to correct images for geometric effects (Lucht, 2000; Roujean, Leory, & Deschamps, 1992; Wanner, Li, & Strahler, 1995; Wanner et al., 1997). Although these models are effective in correcting images for viewing geometry effect and for understanding the radiative transfer processes, simplified and more flexible methods may be useful for operational corrections of this effect.

Recent advances in neural network and artificial intelligence may provide an alternative to traditional equation-based BRDF models. For example, the neural fuzzy inference system (FIS), which uses a neural network to train an FIS (fuzzy inference system), has been used in land-use and land-cover classification of remotely sensed imagery and proved to be more accurate than traditional unsupervised or supervised classification techniques (Gopal, Woodcock, & Strahler, 1999). Fuzzy inference systems (FIS) are not constrained by the rules of traditional equations, are very good at discerning complex patterns, and can be easily modified with additional inputs. However, understanding the physical processes being modeled is difficult compared with BRDF models. Visualization tools are useful for looking at the relationships between variables in an FIS, which may provide some insights into the physical processes. The main objective of this study was simply to test whether an FIS can be used as an alternative for correcting viewing geometry effects. A secondary objective is to test the robustness of an FIS in comparison to traditional BRDF models. A more detailed description of FIS is given in Appendix A. This comparative analysis was made with one set of ground-based data and two sets of aircraft-based data as described below.

2. Study sites and data sets

Two study sites were used, one in Shafter, CA and one in Lubbock, TX (Table 1). At the Texas site, two data sets were collected: one set of ground-based measurements and one set of aircraft-based measurements. Both study sites were the locations of experiments conducted by Resource21, a Denver-based remote sensing company.[1] The site in Texas was the location of an experiment investigating the influence of water and nitrogen on the reflectance properties of agricultural crops. The site in California was a study site for an experiment in determining crop planting densities from remotely sensed data.

Solar zenith angle is an important variable in BRDF analysis. The influence of this variable was significant only for our ground data in the Texas data set, where measurements were taken over a period of 1 hour. For the Texas aircraft data set, the change in solar zenith angle was minimal because the six images used in the analysis were acquired within 15 min of each other on the same day. The solar zenith angle ranged from 35° to 38° for the six images so its effect was considered negligible. The analysis of the California data set consisted of just one image where the solar zenith angle was constant. For both aircraft data sets, we treated the solar zenith angle as a constant. For the Texas ground data, solar zenith angle was included in the analysis, although the FIS performed just as well when the solar zenith angle was held constant.

For our ground-based study in Texas, we used a 12.19×12.19-m (40×40-ft) research plot (plot number 143 in Fig. 1) of cotton to measure the reflectance at different viewing angles and solar azimuths. This was done with an apparatus that allows the mounting of a radiometer on the top of a boom for measuring surface reflectances at different viewing angles (Jackson et al., 1990). By turning around the base of the apparatus, we were also able to make measurements at a range of solar azimuth angles.

The radiometer used for this study was a four-band Exotech sensor, with blue, green, red, and near-infrared (NIR) filters corresponding to the first four spectral bands of the Landsat TM sensors. The Exotech measured an area on

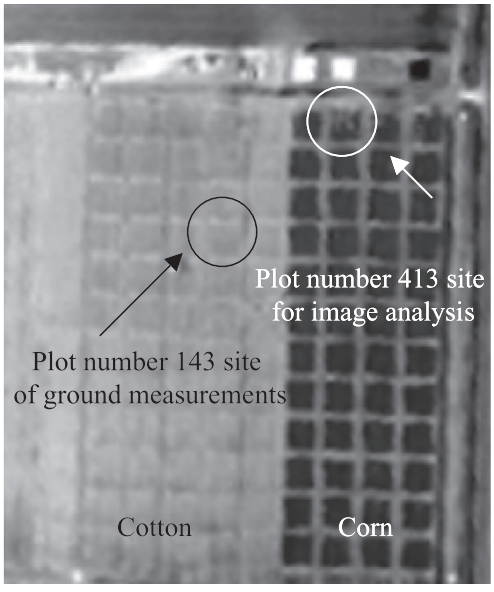

Fig. 1. Image of the study site in Lubbock, TX for both ground-based and aircraft-based data. Plot numbers 143 and 413 are from original experimental design.

[1] The use of company names and brand names are necessary to report factually on available data; however, the USDA neither guarantees nor warrants the standard of the product, and the use of the name by USDA implies no approval of the product to the exclusion of others that may also be suitable.

the ground approximately 1 m in diameter when the sensor is viewing at nadir angle. At a 45° viewing angle, the footprint will be an oval with a long axis of 2.8 m and a short axis of 1 m. This is different from the geometry of a view zenith angle in an image since image pixels are rectangular. The viewing geometry effects acquired from our ground data cannot be directly translated to effects observed from aerial imagery because our sensor device for data acquisition did not precisely duplicate the viewing geometry for that environment The measurements were taken on July 20, 1998 from 8:00 to 9:00 a.m. local time. The cotton cover at the time of measurements was approximately 50% (canopy was still under development). Because of the row/furrow structure of the cotton fields, at each scanning plane, three rows and three furrows were measured (row spacing, 1.02 m or 40 in.). The sensor was placed over a row first, and a scan reading was taken. Then, the sensor was moved over a furrow, and the reading was repeated. This was repeated three times. In the post-processing, all data for each scanning plane were separated by row and furrow and then sorted according to view zenith angles. The measurements were binned at 5° intervals and averaged. The average of all the rows and all the furrows were averaged for each 5° bin for a final value for the viewing angle at the center of the bin. This resulted in a set of reflectance measurements from nadir to 70° at 5° intervals and at five different relative azimuths, 0°, 45°, 90°, 135°, and 180°. This was an attempt to acquire an average of the view angle effect of the reflectance of a cotton canopy. It should be emphasized that the row furrow structure of the cotton canopy greatly complicates view angle effects. The average values we analyzed are not expected to be valid for other row furrow structure of cotton.

The second data set from the Texas site was from aircraft images. The Resource21 aircraft imager was flown over the experimental site along several different flight directions to collect data at different view zenith angles. The images were acquired at approximately 305 m above ground level (AGL) on June 26, 1998 with a 12-bit digital camera filtered to four spectral bands. Band widths were 0.45–0.52, 0.52–0.60, 0.63–0.68, and 0.775–0.90 μm. Ground resolution was approximately 0.52 m, and the image consisted of 1025×1025 pixels with a field of view of 28.6°. This resolution was not ideal for analyzing view angle effects because geometric effects are best analyzed when image resolution is much larger (10 times or more) than the structures in the image since geometric effects are traditionally considered mixed pixel effects of object and shadow. We did not degrade the image resolution because it would have reduced the number of pixels available for data analysis for one plot. Our results are presented as an average of the entire plot. We chose to analyze one 12.19×12.19-m plot (plot 413, Fig. 1) because it occurred at the center of one of the images corresponding to a nadir view angle. This particular plot was captured in five other images at different locations in the image giving us a total of six images for analysis. In this study, we analyzed the near-infrared band (NIR) of six images of the experimental plot number 413 (Fig. 2). Twenty values from each image of plot 413 were randomly extracted,

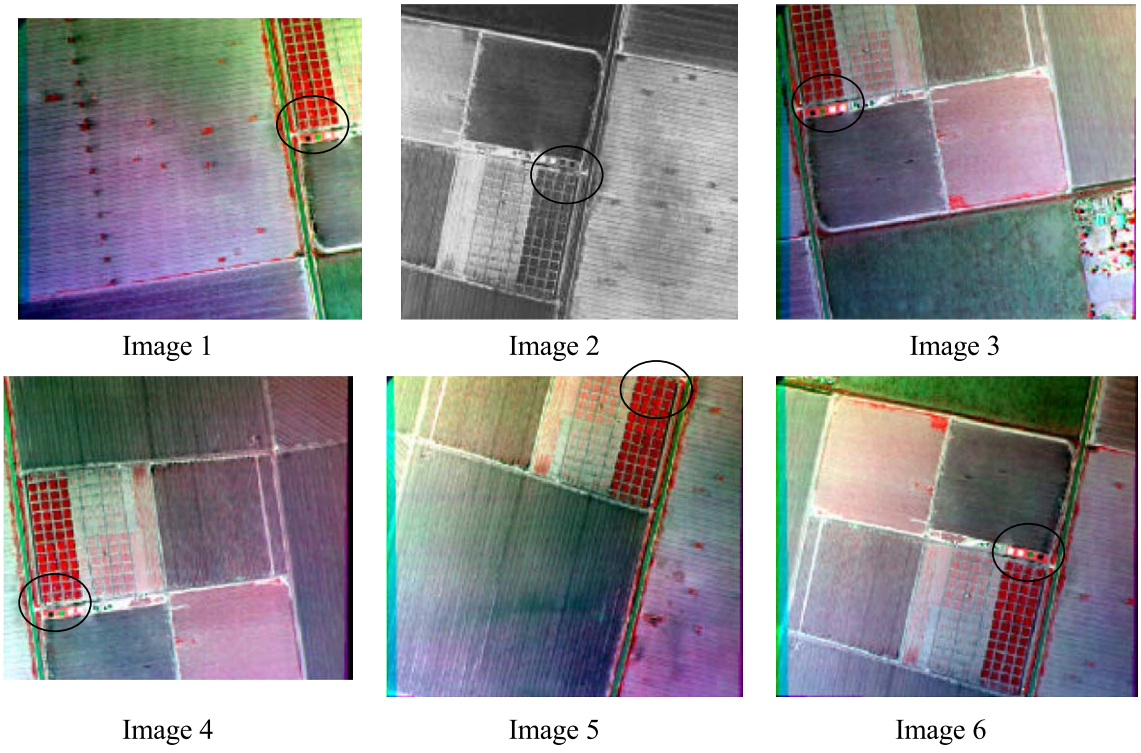

Fig. 2. Set of images used for Texas aircraft data analysis. Circles indicate locations of study site in each image.

totaling about 5% of the total number of pixels in the plot. The values extracted were unprocessed digital numbers. Since all images were acquired within 15 minute and no changes were made to the controls of the camera, post-processing was not necessary for the investigation of relative viewing geometry effects. In addition, the low altitude of image acquisition as well as the constant clear atmosphere at the time of acquisition allowed us to neglect confounding atmospheric effects.

The second study site was in Shafter, CA at the USDA Cotton Research station. The field was split up into 16 equal plots (12×90 m) for a plant density experiment. The plots were designed in a 4×4 randomized block (Fig. 3). Treatment plant densities were 10, 20, 30, and 50 thousands of plants/acre. The plots were planted with Acala (MAXXA) cotton on April 18, 1997 and emergence occurred on April 24, 1997.

An aircraft was flown at 305 m AGL on May 27, 1997 to acquire the image used for the Shafter study. The sensor was the same as that used at the Texas study site, with a resolution of 0.5 m.

The Shafter data set was analyzed to see if the viewing geometry would influence the interpretation of planting densities of newly emerged cotton in a relatively small area of an entire aircraft image. First, we examined the original image to establish whether viewing geometry effects were significant. Since the replicates were randomized, no plots of the same planting density were adjacent to each other. The planting densities and crop conditions were precisely controlled and monitored so it could be assumed that each repetition would have a very similar average digital number (DN) value in the near-infrared band image, which is very sensitive to the presence of green vegetation. If the DN values for each replicate had a relationship to the plot location, then most likely, this relationship would be the result of viewing geometry effects.

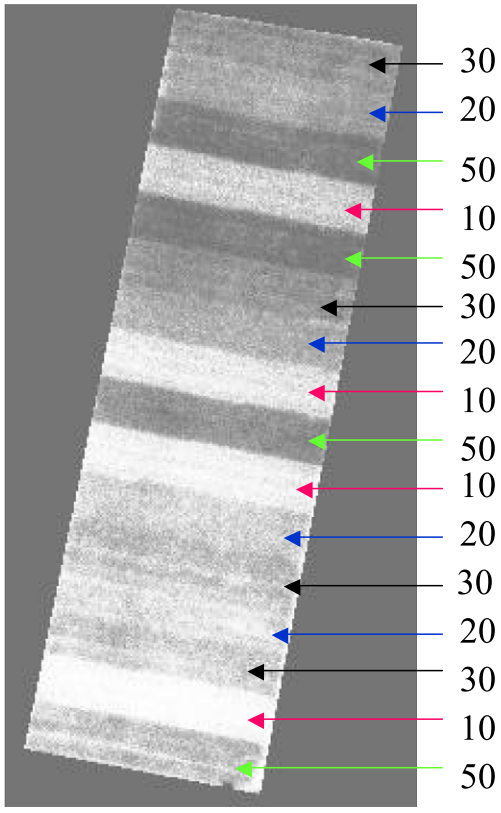

Fig. 3. Image of the plant density study of cotton in Shafter, CA. Numbers refer to thousands of plants per acre planted. The image was acquired on May 27, 1997, shortly after emergence.

3. Methodology: model and FIS descriptions

Earlier research showed that equation-based BRDF models were able to predict values from data acquired on the ground with reasonable accuracy using only viewing zenith and view azimuth angles as inputs (Cabot, Qi, & Moran, 1994; Lucht & Roujean, 2000; Strahler, 1997). This study investigated whether a simple FIS would work as well or better than the traditional BRDF models. To do this, we selected three BRDF models, one from each of the physical, semiempirical, and empirical categories. Equation-based models simulate BRDF properties reasonably well for a homogeneous surface. Previous research (Cabot et al., 1994; Dymond & Qi, 1997; Lucht & Roujean, 2000) has shown that the Shibayama and Wiegand (1985, empirical), Roujean et al. (1992, physical), and Dymond and Qi (1997, semiempirical) models suitably describe a BRDF function for agricultural crops when used with appropriate coefficients (see Appendix A for descriptions). We chose these three BRDF models and developed one fuzzy inference system (FIS) model for comparison with the ground data. The mathematical expressions of these three models are provided in Appendix A.

The fuzzy inference system (FIS) used in this study is a set of rule-based logics. An FIS takes input variables and, instead of developing an equation, creates membership functions for each variable. Rules are then created that evaluate the membership functions to result in a single output value. When an FIS is optimized or trained, the rule and membership functions are adjusted to best fit the training data set. Appendix B provides a brief description and example of the development of rules and membership functions.

4. Methodology: ground-based data

The BRDF models were first run in an inverse mode to optimize the model parameters. The optimization routine used to train the equation-based BRDF models was the simplex procedure (Nelder & Mead, 1965). The FIS was developed and trained at the same time using an adaptive neuro-fuzzy inference system (ANFIS). Once the models (both BRDF and FIS) were optimized, they were used to simulate the spectral reflectances. The simulated reflectances

were then compared with ground data using graphic presentation and statistical measures.

5. Methodology: aircraft-based data

The successful prediction of values with the BRDF models and an FIS ideally requires a complete data set of view zenith angles, a uniformly distributed set of relative azimuth angles, and measurements of the same area on the ground for training of the FIS and BRDF models. Aircraft-based images are rarely suitable for this kind of analysis because, in many cases, the area of interest is only a part of the image and therefore has a limited range of viewing angles. Even if the entire image is of interest, different parts of the image would most likely contain different objects with very different view zenith angle properties, which would require that the image be split up into subsections for correction of viewing geometry effects. In a case like this, both the equation-based BRDF models and the FIS would predict an overall average BRDF for the image.

In most aircraft images, there is a tremendous variability in pixel values unrelated to viewing geometry effects. The 120 randomly extracted values (20 values from each image) from the Texas images were plotted (grouped by image) in the order in which they were extracted (Fig. 4). Two sources of variability were apparent: (1) variability between each pixel value and (2) an overall variability between images which is the variability due to differences in view zenith angle and relative azimuth of the plot. This was assumed because the only difference between the six images of the same plot was viewing geometry. If the BRDF models were to predict values based only on geometric inputs (i.e., view zenith angle and relative azimuth), then the heterogeneity due to other factors (i.e., differences in LAI, soils, etc.) would not be included in the model prediction, making the predicted values less accurate. In BRDF models, this is considered noise because the models are not designed or expected to predict this variability (Lucht, 2000). This is true for an FIS as well, which explains the poor fit between values predicted by the FIS and the values used to train the FIS (Fig. 5). The variation within the predicted values (Fig. 5) was caused by viewing geometry. The FIS model created a best fit based on the input values by averaging variation of the data set due to other factors. The only inputs were viewing geometry inputs, so the FIS did not have access to other sources of variation; therefore, they were ignored by the FIS. If the model predicted the values exactly, then all of the variation in the data set would be due to viewing geometry effects, which we know is not the case. The equation-based models do essentially the same thing. The primary difference is that the fit is constrained to a certain extent by the equation where the ANFIS seeks a pattern that fits the input parameters, in this case, the viewing geometry. We illustrate this effect in the results section of the ground data.

To correct for viewing geometry effects in this image, only the variation in the predicted value from the model needs to be removed from the original value. With equation-based BRDF models, this is accomplished by predicting a value with the equation set to some standard geometry, (usually, view zenith angle equals zero and solar zenith angle equal to that of the time of image acquisition), making a second prediction of the pixel value at the actual viewing geometry and then calculating the ratio of these two values. This result is a correction coefficient that is multiplied by the original value to correct for the BRDF effect.

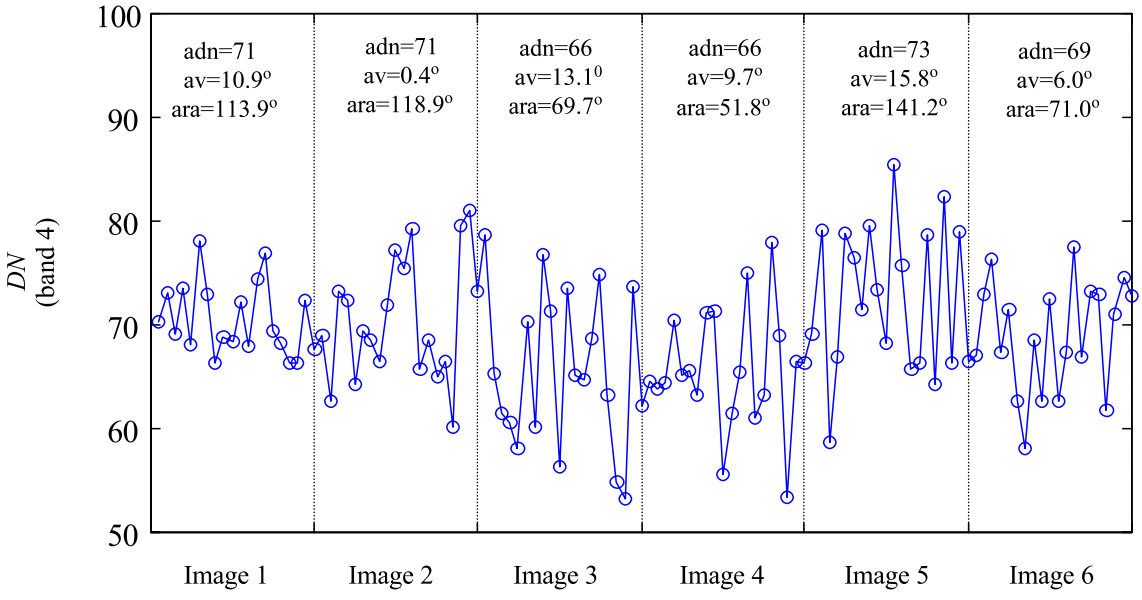

Fig. 4. Randomly selected data values from Texas aircraft images. Image numbers correspond to image numbers in Fig. 3, where: adn=average dn, av=average view zenith angle, and ara=average relative azimuth.

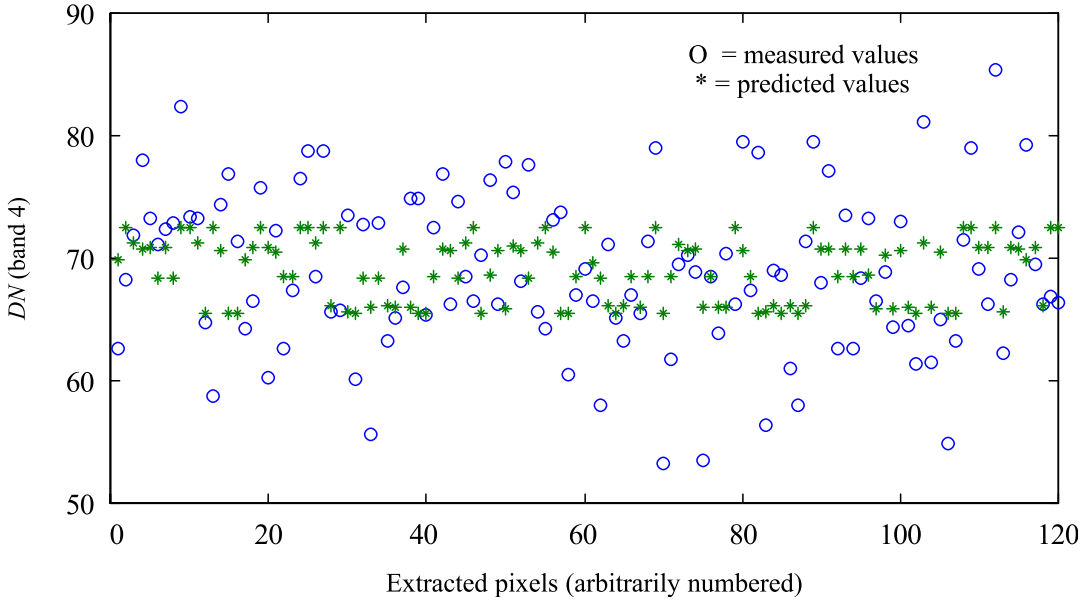

Fig. 5. Randomly selected data values from Texas aircraft images (circles). Values predicted by an FIS after being trained with measured values shown (asterisks).

Since the FIS is not equation based, it can only predict geometric effects within the bounds of the data that was used to train the FIS. In order to correct for geometric effects in the manner described above, the training data must include values at or close to a view zenith angle of zero. The lowest view zenith angle in the Texas aircraft data set was 0.12°, which is the value we used with the FIS to correct for viewing geometry effects. Unfortunately, because we were only using a part of an image for the California aircraft data, our lowest view zenith angle was 2.1°. For demonstration purposes, we simply calculated the ratio of the lowest value predicted by the FIS to the value

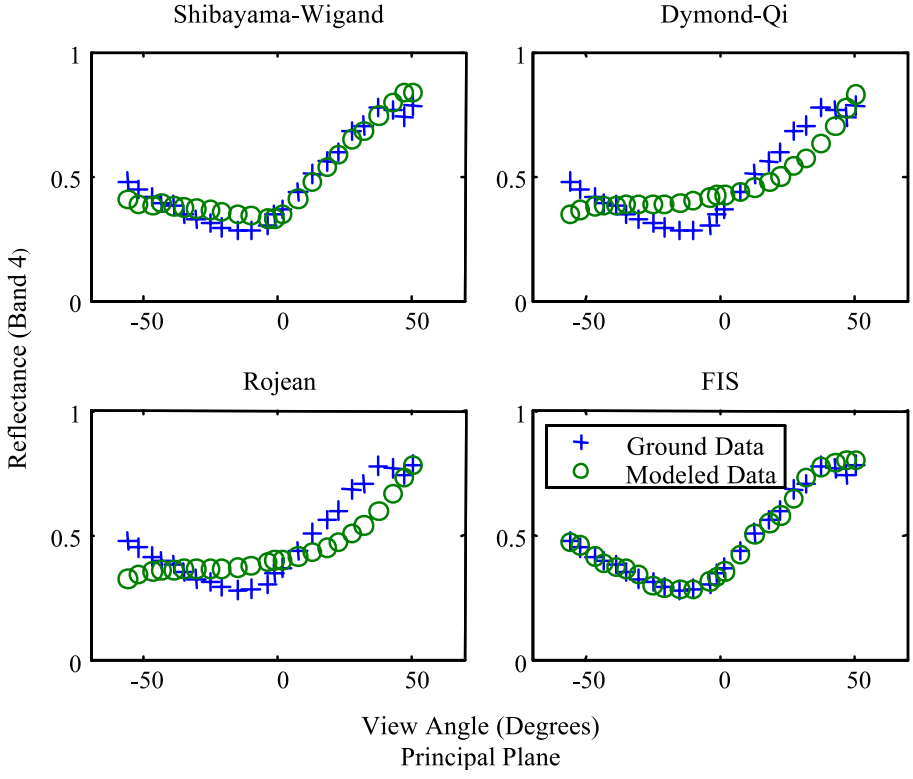

Fig. 6. Comparison of different models in the principal plane (band 4) for prediction of reflectance from Texas ground-based data.

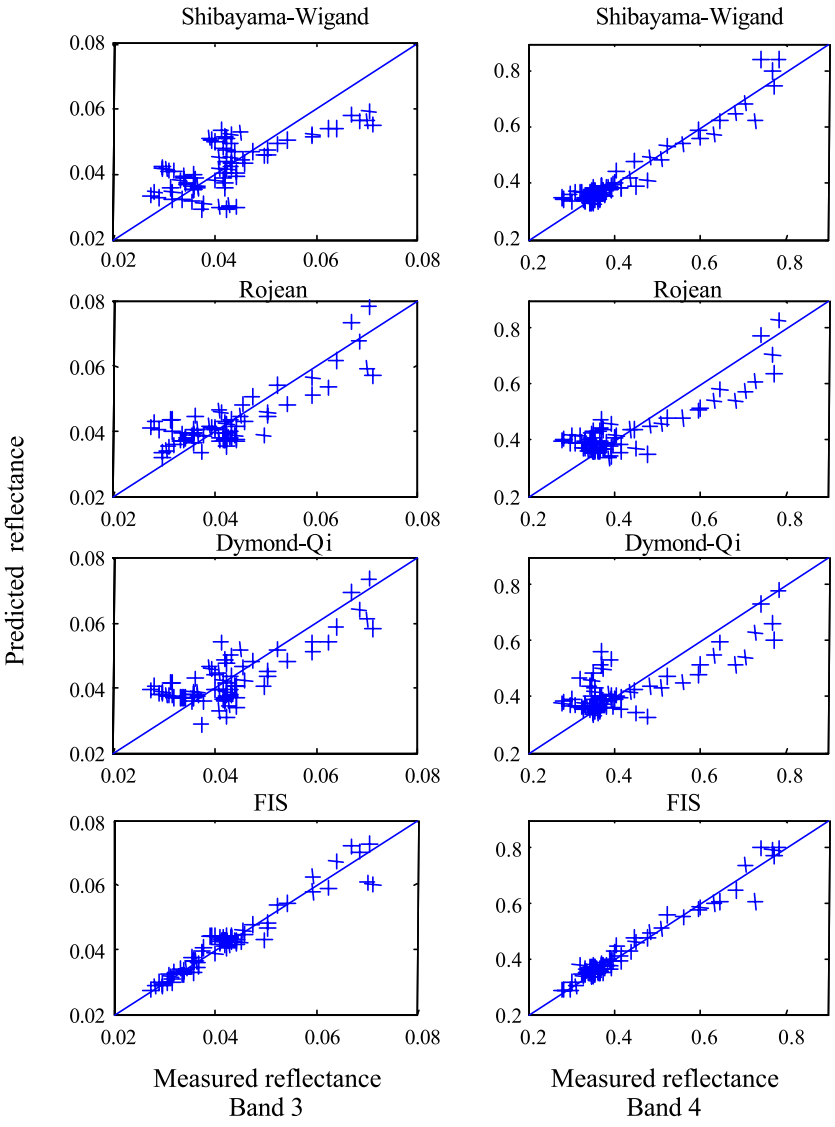

Fig. 7. Comparison of different models for prediction of reflectance from Texas ground-based data.

predicted for the viewing geometry of the image for the correction coefficient. This corrected for relative differences due to geometric effects but not for absolute differences.

6. Results

Because the three data sets used in this study had very different characteristics and the methodology used for the ground-based data varied somewhat from that of the aircraft-based data, the results are presented separately for each data set.

6.1. Results A: Texas ground data

After all the models were optimized, ground-measured data in the principal plane (relative azimuth 0° and 180°) were compared to the predicted data for all four models in band 4 (Fig. 6). The principal plane was chosen because viewing geometry effects are greatest in this relative azi-

Table 2
Statistical merit of regression and root mean square error (RMSE), actual vs. predicted reflectance for spectral bands 3 and 4

Model	R^2 (band 3)	RMSE (band 3)	R^2 (band 4)	RMSE (band 4)
Shibayama–Wiegand	0.530	0.0054	0.934	0.0317
Roujean	0.681	0.0049	0.779	0.0451
Dymond–Qi	0.643	0.0051	0.664	0.0539
FIS	0.937	0.0026	0.965	0.0234

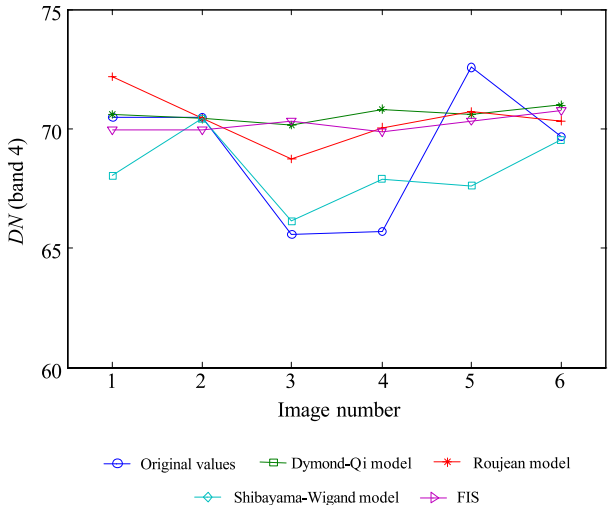

Fig. 8. Average reflectance values of randomly selected data points for the Texas aircraft images before and after correction for viewing geometry effects. Image numbers correspond to image numbers in Figs. 2 and 4.

muth plane. Fig. 6 illustrates the advantage of using a model to predict viewing geometry effects that is essentially an empirical "pattern finder." The FIS model was able mimic a viewing geometry effect extremely well. The Shibayama–Wiegand model fit the ground data best out of the equation-based models. The Roujean and Dymond models exhibited very similar results. Secondly, the ground-measured data were plotted against the data predicted by each model (Fig. 7). Regression equations, the statistical R^2, and root mean square error (RMSE) were also calculated (Table 2). The RMSE between band 3 and band 4 varied by an order of magnitude because of the difference in the range of reflectances in the bands (0.03–0.07 for band 3 and 0.28–0.78 for band 4). Therefore, the following discussion is limited to the R^2 statistic.

The models' performance varied significantly with R^2 values ranging from 0.53 to 0.96. The Shibayama–Wiegand model was able to predict the near-infrared (band 4) much better than the red (band 3) (R^2=0.93 versus R^2=0.53). The Roujean and Dymond–Qi models performed better for band 4 (R^2=0.78) than band 3 (R^2=0.66). The FIS performed the best for both bands with an R^2=0.94 and 0.97 for bands 3 and 4, respectively. For this data set, it is apparent that the FIS is a better model for predicting reflectance based on relative azimuth and view zenith angles. This is because the

Table 3
Average values for 20 randomly extracted pixels from each image

Model	Image 1	Image 2	Image 3	Image 4	Image 5	Image 6
Uncorrected	70.5	70.5	65.6	65.7	72.6	69.7
Dymond–Qi	68.0	70.4	66.1	67.9	67.6	69.6
Roujean	72.2	70.5	68.8	70.1	70.7	70.3
Shibayama–Wiegand	70.6	70.4	70.2	70.8	70.6	71.0
FIS	70.0	70.0	70.4	69.9	70.4	70.8

Table 4
Standard deviation for all six images after correcting for viewing geometry effects

Model	Dymond–Qi	Roujean	Shibayama–Wiegand	FIS
Standard deviation	1.5	1.0	0.3	0.3

FIS model is basically a curve-fitting algorithm with almost no functional restrictions, while the BRDF models are based on fixed forms (equations). The membership functions and flexible function coefficients made the FIS more flexible to fit the BRDF properties (shapes) of heterogeneous surfaces like ours.

6.2. Results B: Texas aircraft data

Recall that the Texas aircraft data and the California aircraft data were not processed beyond the digital number before being corrected for geometric effects. The Texas data was analyzed by plotting the average of the 120 values from each of the six images sequentially before and after viewing geometry correction (Fig. 8; Tables 3 and 4). The Shibayama–Wiegand model and the FIS were very effective in removing variation that was caused by different viewing geometries as evidenced by the constant average value for all the images after the correction was made. The Dymond–Qi and the Roujean models reduced the viewing geometry effect but not completely.

6.3. Results C: California aircraft data

Data from the California study site exhibit a relationship between the viewing geometry and the DN value for each planting density (Fig. 9). As relative azimuth and viewing angle decreased, the DN values increased. This suggests that the relative azimuth effects overwhelmed the view zenith angle effects since the view zenith angles did not vary significantly. The trends in DN in relation to viewing geometry were not tested for statistical significance.

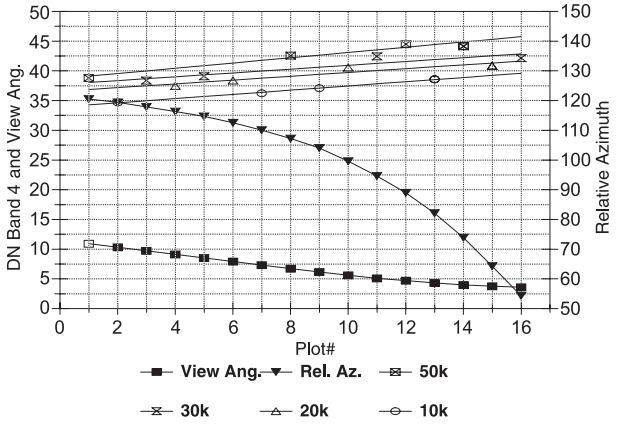

Fig. 9. DN values of band 4 of the Shafter study site before correcting for viewing geometry effects, separated by treatment density.

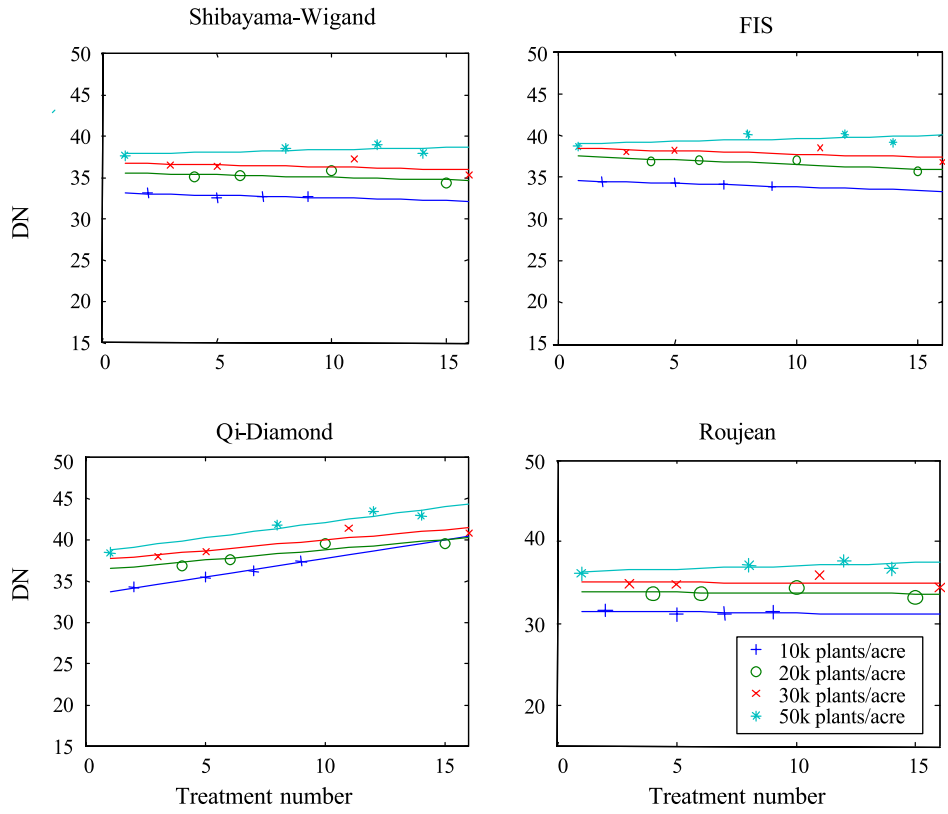

Fig. 10. DN values of band 4 of the Shafter study site after correcting for viewing geometry effects, separated by treatment density. The legend designations of 10k, 20k, 30k, and 50k are plant treatment densities (thousands of plants/acre).

After obtaining correction coefficients from each BRDF model and the FIS, we corrected the entire image (Fig. 10). The spatially dependent trend of the DN values for each plant density was removed, yet the different densities were still separable, demonstrating that the value of the DN due to plant density had been preserved, but the difference in DN values due to viewing geometry had been removed. The Roujean and the Shibayama–Wiegand models removed viewing geometry effects equally well as demonstrated by similar slope values of the trend lines for all the planting densities (Table 5). Results for the FIS model exhibited a slightly greater downward trend for the low plant densities and a slightly upward trend for the highest plant density. The Dymond–Qi model shows a significantly greater upward trend, which was the trend of the original data (Fig. 9) from the uncorrected image. Note that this analysis assumed that the average values of the plots of the same densities were equal. If the plots with higher numbers were actually less dense, due to soil conditions, for example, then the FIS would have made the best correction. Similarly, if for some reason the higher numbered plots were actually denser than the lower numbered plots, then the Dymond–Qi model would have made the best correction. Unfortunately, ground-based data were not available for comparison with the image data to confirm this. The plant densities varied by experimental design in the image analyzed; the image was acquired only 4 weeks after plant emergence so the range of DNs in the image is narrow (33–48). If the image had included plots with full cover, the models tested may have behaved differently. We did not perform a statistical analysis on the separatability of the different plant densities, but before correction, the obvious spatial correlation between different plots of the same density was removed.

Table 5
Slope of trend line for different planting densities of experimental plot after correcting for viewing geometry effects

Planting density ($\times 10^3$)	Dymond–Qi	Roujean	Shibayama–Wiegand	FIS
10 plants/acre	0.439	−0.064	−0.060	−0.064
20 plants/acre	0.251	−0.060	−0.060	−0.060
30 plants/acre	0.254	−0.054	−0.055	−0.053
50 plants/acre	0.375	0.050	0.052	0.050

7. Concluding remarks

For the data sets examined in the study, the FIS performed as well or better than the equation-based BRDF models. Most traditional BRDF models are based on

extensive research and validation. Therefore, they are a useful tool for studying the geometric effect on radiative transfer processes. In addition, the possibility of the equation-based BRDF models yielding unreasonable results is minimal. On the other hand, an FIS is simply fitting to a pattern based on given inputs. This raises the possibility of an FIS model that fits the data training set extremely well but makes little physical sense. The likelihood of this is low because, given only viewing geometry inputs, the chances of other factors actually having a relationship to viewing geometry data is very small. If there were no relationship to viewing geometry inputs and pixel value, the FIS would simply fail to create a pattern. Additionally, because FIS is not constrained to correcting only for viewing geometry effects, the possibility exists that effects from the atmosphere and inherent sensor and experimental error are also being corrected by the FIS. Should these effects be correlated with the geometric variables that were input to the FIS, this would indeed be the case. We are not implying that the FIS is a valid or appropriate replacement for rigorous, physically based BRDF models. We have shown that an FIS is very effective at finding patterns based on inputs that are known to have a complex but ultimately predictable effect on the data. This research is highly experimental. The practical usefulness of FIS for correcting geometric effects remains a topic of future research. Further research might include extending an FIS or adding other mathematical models to extrapolate from the given training data, extensive testing on different data sets to evaluate the usefulness of an FIS that is not site or image specific, investigating the correlation of geometric effects with other biophysical effects by inputting additional variables to the FIS, and additional comparisons of FIS to proven, physically based, BRDF models.

The advantage of fuzzy inference systems is that they provide greater flexibility than traditional equation-based BRDF models for describing observed BRDF patterns with many dependent variables in terms of finding a pattern to given inputs. In addition, unlike neural networks, the mathematical components that make up an FIS are easily accessible. This allows a user to analyze the system to insure that the relationships described in the FIS do not contradict already established relationships. In addition, an FIS can easily be extended with additional inputs and membership functions to account for more complex data sets or patterns. Although we used the Matlab FIS toolbox (Matlab, 1998), FIS is not a proprietary algorithm and could be built with any programming language. We hope this paper will encourage more researchers in the natural sciences to investigate this useful tool.

Acknowledgements

We would like to thank Resource21 for their generous support of this project. We would also like to thank Dr. Don Wanjura and Dr. Dan Upchurch from USDA-ARS at Lubbock, TX for their support, as well.

Appendix A. Brief description of fuzzy inference systems

The reader is referred to Jang, Sun, and Mizutani (1996) for a complete discussion of fuzzy and neuro-fuzzy theory. In this section, a few terms are defined to explain our approach. Instead of equations with coefficients that are optimized, an FIS has rules associated with the independent variables and membership functions that define how the rules act on the data. It is the membership functions that are optimized. Membership functions usually have a mathematically defined shape with parameters that can be adjusted to change the shape. For example, a Gaussian membership function has the shape

$$y = e^{\frac{-(x-c)^2}{2\sigma^2}}, \tag{A1}$$

where c and σ are the parameters that adjust the shape of the function. The x-axis of a membership function is the range of an independent variable for the FIS. In this study, one independent variable was view angle which ranged from 7° to 12° in the California data set. The y-axis always ranges from 0 to 1 and defines how well an x value fits a particular membership function. A view angle of 7° would have a membership function value of 0.19 for the Gaussian membership function in Fig. A1. In this particular example, c=5 and σ=0.01.

The user developing the FIS chooses the number of membership functions for each independent variable. For this FIS, two membership functions were chosen for each variable because adding additional membership functions did not improve the accuracy of the FIS. Each function has a generalized bell shape as described below.

$$y = \frac{1}{1 + \left|\frac{x-c}{a}\right|^{2b}} \tag{A2}$$

Parameters a, b, and c are adjusted by the adaptive neuro-fuzzy interface system (ANFIS) to fit the output data.

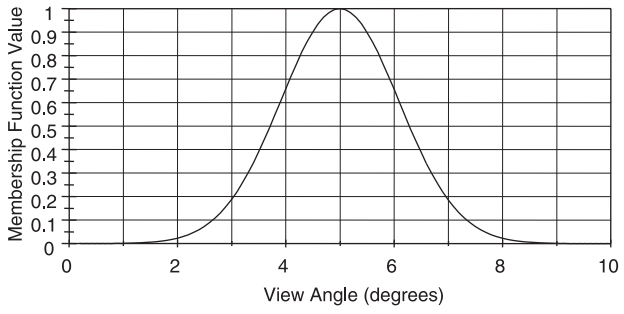

Fig. A1. Example of a Gaussian membership function for a range of view zenith angles.

For the California data set, the two independent variables trained against the data were relative azimuth and view angles. Since we were correcting just one image, the solar zenith angle remained constant but could be used as another variable when analyzing multiple images with different solar zenith angles.

Every independent variable in the FIS has its own set of membership functions. In this model, two membership functions were chosen for view angle and relative azimuth and labeled low and high view angle and low and high relative azimuth. The membership functions are commonly given descriptive names for clarity (i.e., high, low). Fig. A2 illustrates these functions. For a pixel with a relative azimuth of 100° and a view angle of 6, the membership function values are as follows:

value for relative azimuth membership function: low= 0.3
value for relative azimuth membership function: high= 0.7
value for view angle membership low= 0.65
value for view angle membership function: high= 0.35.

These values represent the degree to which the independent variable is a member of the membership functions.

The second part of an FIS is a set of "if, then" rules that essentially define the 'endmember' of an input value (independent variable), that is when the when a particular membership function value equals 1. The value of the predicted variable for each 'endmember' is determined through the ANFIS. In other words, it is part of the optimization procedure.

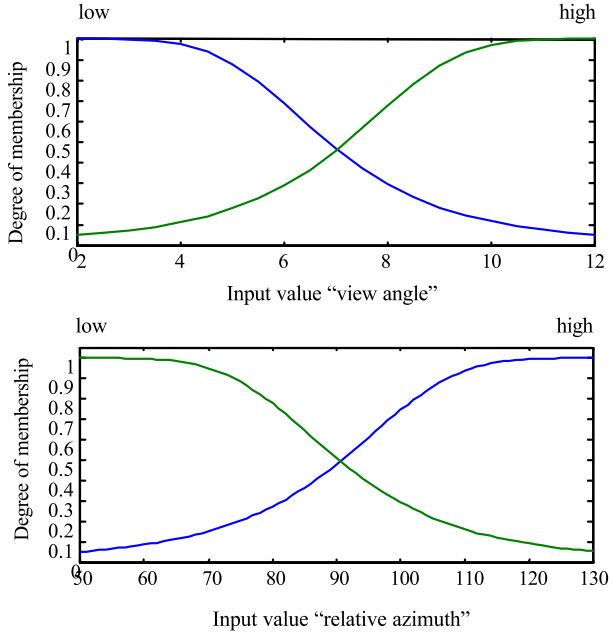

Fig. A2. Example of membership functions for input values "view zenith angle" and "relative azimuth."

1. If view angle is low and relative azimuth is low, then predicted DN is 36.6
2. If view angle is low and relative azimuth is high, then predicted DN is 40.5
3. If view angle is high and relative azimuth is low, then predicted DN is 42.8
4. If view angle is high and relative azimuth is high, then predicted DN is 42.7.

The values in the "if, then" rules are combined with the membership values to get one predicted value for each input value (independent variable) For this particular model, application of the "and" rule requires that the values obtained from each membership function in the rule be multiplied to get one membership value for each rule. Then, the sum of the predicted values is calculated to derive a single output value for a set of inputs (dependent variables) (Eq. (A3)). The values from our example yield

$$\begin{aligned}\text{predicted value} = {} & (0.3 \times .65 \times 36.6) + (0.65 \times 0.7 \times 40.5) \\ & + (0.3 \times 0.35 \times 42.8) \\ & + (0.7 \times 0.3 \times 42.7) \qquad \text{(A3)}\end{aligned}$$

$$\text{predicted value} = 40.52.$$

This is the Sugeno type of FIS. Another type of FIS is the Mamdani, where the output values are actually membership functions that are then converted into a single output number.

As with traditional models, an FIS needs to be trained with a data set from the image to be corrected. It is not possible to train an FIS with traditional optimization methods, so we used an adaptive neuro-fuzzy inference system (ANFIS) developed by Jang et al. (1996). An ANFIS is given a set of variables upon which the output data set is dependent. Membership functions are created for each variable, and the functions are trained to best fit the output data. It is the ANFIS that performs the iterative process that adjusts the membership function parameters using a combination of a back-propagation algorithm and the least squares method.

Appendix B. BRDF models used

(1) Shibayama–Wiegand (1985) model

$$\rho(\theta_s, \theta_v, \varphi) = R_0\left[1 + \left(\beta_0 + \beta_1 \sin\left(\frac{\varphi}{2}\right) + \frac{\beta_2}{\cos\theta_s}\right)\sin\theta_v\right] \qquad \text{(A4)}$$

where ρ=reflectance factor; θ_s=solar zenith angle; θ_v=view angle; φ=relative azimuth; R_0=nadir reflectance factor; β_0, β_1, β_2=empirical parameters.

(2) Dymond–Qi (1997) model

$$L = S(\theta,\phi)H(\alpha,\phi)B(\alpha) \tag{A5}$$

where

$$S(\theta,\phi) = \frac{\cos\theta}{\cos\theta + (\sigma_\theta/\sigma_\phi)\cos\phi} \tag{A6}$$

$$H(\alpha,\theta) = \begin{cases} 2\exp(-\tan(\alpha/2)/h\theta) & \alpha < \pi/2 \\ 2\exp(-\tan(\pi/4)/h\theta) & \alpha \geq \pi/2 \end{cases} \tag{A7}$$

$$B(\alpha) = \frac{4\rho E}{3\pi^2}(\sin\alpha + (\pi/2 - \alpha)\cos\alpha) \tag{A8}$$

θ=sun zenith angle; ϕ=off-nadir view angle; α=phaseangle; σ_θ=average projected leaf area in the sun direction; σ_ϕ=average projected leaf area in the view direction; h=constant which is proportional to the length divided by the distance between leaves; ρ=leaf reflectance; E=radiant flux density of the sunlight; L=canopy radiance.

(3) Roujean (1992) model

$$\rho(\theta_s,\theta_v,\varphi) = k_0 + k_1 f_1(\theta_s,\theta_v,\varphi) + k_2 f_2(\theta_s,\theta_v,\varphi) \tag{A9}$$

$$f_1(\theta_s,\theta_v,\varphi) = \frac{1}{2\pi}((\pi-\varphi)\cos\varphi + \sin\varphi)\tan\theta_s\tan\theta_v - \frac{\tan\theta_s + \tan\theta_v + G}{\pi} \tag{A10}$$

$$f_2(\theta_s,\theta_v,\varphi) = \frac{4}{3\pi}\frac{1}{\cos\theta_s + \cos\theta_v} \times \left(\left(\frac{\pi}{2} - \xi\right)\cos\xi + \sin\xi\right) - \frac{1}{3} \tag{A11}$$

$$\cos\xi = \cos\theta_s\cos\theta_v + \sin\theta_s\sin\theta_v\cos\varphi \tag{A12}$$

$$G = \sqrt{\tan^2\theta_s + \tan^2\theta_v - 2\tan\theta_s\tan\theta_v\cos\varphi} \tag{A13}$$

where ρ=surface reflectance; θ_s=solar zenith angle; θ_v=view angle; Φ_r=relative azimuth; ρ_0=surface background reflectance; f_1, f_2=analytic functions of the solar zenith angle and view angle; h=average height of surface protrusions; l=average spacing of surface protrusions; ω=single leaf scattering albedo; τ=optical depth of the foliage of the canopy.

References

Asrar, G., & Myneni, R. B. (1992). Application of radiative transfer models for remote sensing of vegetation conditions and states. In Myneni, & Ross (Eds.), *Photo-vegetation interactions: Applications in optical remote sensing and plant ecology* (pp. 537–558).

Cabot, F., Qi, J., & Moran, M. S. (1994). Test of surface bi-directional reflectance models with surface measurements: Results and consequences for the use of remotely sensed data. *Proceedings of Sixth International Symposium on Physical Measurements and Signatures in Remote Sensing, Jan. 17–21, Val d'Isere, France*.

Deering, D. W., Eck, T. F., & Otterman, J. (1990). Bidirectional reflectances of selected desert surfaces and their three-parameter soil characterization. *Agricultural and Forest Meteorology*, *52*, 71–93.

Dymond, J. R., & Qi, J. (1997). Reflection of visible light from a dense vegetation canopy—A physical model. *Agricultural and Forest Meteorology*, *86*, 143–155.

Gopal, S., Woodcock, C. E., & Strahler, A. H. (1999). Fuzzy neural network classification of global land cover from a 1° AVHRR data set. *Remote Sensing of Environment*, *67*, 230–243.

Hu, B., Wanner, W., & Strahler, A. H. (1997). Validation of kernel driven semiempirical models for the surface bidirectional reflectance distribution function of land surfaces. *Remote Sensing of Environment*, *62*, 201–214.

Jackson, R. D., Teillet, P. M., Slater, P. N., Fedosejevs, G., Jasinski, M. F., Aase, J. K., & Moran, M. S. (1990). Bidirectional measurements of surface reflectance for view angle corrections of oblique imagery. *Remote Sensing of Environment*, *32*, 189–202.

Jang, J., S. -R., Sun, C. -T., Mizutani, E. (1996). *Neuro-fuzzy and soft computing: A computational approach to learning and machine intelligence*. Prentice Hall, pp. 73–90, 333–363.

Kimes, D. S., Sellers, P. J., & Diner, D. J. (1987). Extraction of spectral hemispherical reflectance (albedo) of surface from nadir and directional reflectance data. *International Journal of Remote Sensing*, *8*(12), 1727–1746.

Lucht, W. (2000). Theoretical noise sensitivity of BRDF and albedo retrieval from the EOS-MODIS and MISR sensors with respect to angular sampling. *International Journal of Remote Sensing*, *21*(1), 81–98.

Lucht, W., & Roujean, J. L. (2000). Considerations in the parametric modeling of BRDF and albedo from multiangular satellite sensor observations. *Remote Sensing Reviews*, *18*, 343–379.

Matlab (1998). *Fuzzy logic toolbox*. Natick, MA: The Mathworks.

Nelder, J. A., & Mead, R. (1965). A simplex method for function minimization. *Computer Journal*, *7*, 308–313.

Qi, J., Huete, A. R., Moran, M. S., Chehbouni, A., & Jackson, R. D. (1993). Interpretation of vegetation indices derived from multi-temporal SPOT images. *Remote Sensing of Environment*, *44*, 89–101.

Roujean, J. L., Leory, M., & Deschamps, P. Y. (1992). A bidirectional reflectance model of the Earth's surface for the correction of remote sensing data. *Journal of Geophysical Research*, *97*(D18), 20455–20468.

Shibayama, M., & Wiegand, C. L. (1985). View azimuth and zenith, and solar angle effects on wheat canopy reflectance. *Remote Sensing of Environment*, *18*, 91–103.

Strahler, A. (1997). Vegetation canopy reflectance modeling—Recent developments and remote sensing perspectives. *Remote Sensing Reviews*, *15*, 179–194.

Wanner, W., Li, X., & Strahler, A. (1995). On the derivation of kernels for kernel-driven models of bidirectional reflectance. *Journal of Geophysical Research*, *100*, 21077–21089.

Wanner, W., Strahler, A. H., Hu, B., Lewis, P., Muller, J. P., Li, X., Barker Schaaf, C. L., & Barsnley, M. J. (1997). Global retrieval of bidirectional reflectance and albedo over land from EOS MODIS and MISR data: Theory and algorithm. *Journal of Geophysical Research*, *102*, 17143–17161.